Spectroscopic characteristics of Yb^{3+}:$LiLa(WO_4)_2$ crystal

Xinyang Huang (黄新阳)

Institute of Research on the Functional Materials, Jiangxi University of Finance and Economy, Nanchang 330013, China

**E-mail: xyhuang0202@hotmail.com*

Received April 15, 2010

The spectroscopic characterization and fluorescence dynamics of Yb^{3+}:$LiLa(WO_4)_2$ crystal are investigated. The Yb^{3+}:$LiLa(WO_4)_2$ crystal exhibits a broad absorption and emission spectral bands, large absorption and emission cross sections, and moderate fluorescence lifetime. Blue light emission around 480 nm is observed at 10 K and is demonstrated through cooperative upconversion from the deexcitation of excited Yb^{3+}-Yb^{3+} pairs.

OCIS codes: 140.3613, 160.5690, 300.2140, 300.2530.

doi: 10.3788/COL20100808.0780.

Recently, with the development of high-power InGaAs diode lasers, increasing attention has been paid to the research on Yb^{3+}-doped laser materials. This research was stimulated because Yb^{3+} demonstrates many advantages over other rare earth ions. Yb^{3+} only has two electronic manifolds (i.e., ground-state manifold $^2F_{7/2}$ and excited-state manifold $^2F_{5/2}$) separated by approximately 10000 cm^{-1}. In addition, Yb^{3+} hardly suffers from cross-relaxation, upconversion, concentration quenching, or excited-state absorption because it lacks relevant high-lying excited states. Its quantum efficiency is also very high, greatly lightening thermal loads, and its long fluorescence lifetime is beneficial for storing energy[1,2]. Due to the presence of strong electron-phonon coupling, Yb^{3+} ions have broad absorption and emission bands, offering the possibility of near-infrared tenability and the generation of ultrashort pulses[3−7].

Double tungstate crystals with the general formula $AB(WO_4)_2$ (A = Li, Na, or K, B = rare earth) from a wide variety of inorganic compounds having monoclinic and tetragonal symmetries have recently attracted growing interest. Their structure diversity provides these crystals with excellent physical and chemical properties as laser hosts, such as excellent chemical durability in air atmosphere, large rare-earth ion admittance, and large absorption and emission cross-sections of rare-earth ions in its lattice[3−11]. Yb^{3+}-doped double tungstate crystals with sheelite-type local disorder structure exhibit relatively broad bandwidths, promising to become rare earth laser hosts for applications requiring tunability or ultrashort pulses. For example, Yb^{3+} laser operation has been demonstrated in several crystal hosts: $NaRe(WO_4)_2$ (Re = Y, Gd, and Lu[3−7]). $LiLa(WO_4)_2$, a Li-based double tungstate crystal, possesses no phase transition and can be directly grown from the flux[12−14]. Moreover, the Yb^{3+}:$LiLa(WO_4)_2$ crystal exhibits excellent thermal and spectroscopic characteristics[13,14]. However, to our knowledge, the polarized optical characteristics and upconversion emission of Yb^{3+}:$LiLa(WO_4)_2$ crystal have not been investigated yet, and this may limit the study of the Yb^{3+}:$LiLa(WO_4)_2$ laser. Therefore, this letter is mainly concerned with the polarized spectroscopic characterization and fluorescence dynamics of Yb^{3+}:$LiLa(WO_4)_2$ crystal.

The Yb^{3+}:$LiLa(WO_4)_2$ crystal was grown by the Czochralski method. The growth procedure was similar to those described in Refs. [12,14]. The X-ray diffraction (XRD) patterns were collected using a D/max-rA diffractometer and employing CuK_α radiation (λ = 0.154056 nm) at room temperature. The Yb^{3+} concentration was measured by inductively coupled plasma atomic emission spectrometry (ICP-AES).

The sample, with the dimension of 5 × 5 × 0.5 (mm), was cut along the [001] orientation from the as-grown Yb^{3+}:$LiLa(WO_4)_2$ crystal and polished for spectroscopic measurement. According to the tetragonal characteristic of lattices, the experimental spectra were labeled as σ or π, defined in terms of the **E**-vector being perpendicular and parallel to the optical axis c, respectively. Polarized absorption spectra were obtained using a Perkin-Elmer ultraviolet-visible-near infrared (UV-VIS-NIR) spectrometer (Lamada-900) in the range of 800 – 1100 nm at room temperature. Emission spectra and fluorescence decay curves were recorded on Edinburgh Instruments FLS920 spectrofluorimeter equipped with both continuous (450 W) and pulsed xenon lamps. For low-temperature measurements, the sample was mounted on a closed cycle cryostat (4-350 K, DE202, Advanced Research Systems).

The XRD pattern of as-grown Yb^{3+}:$LiLa(WO_4)_2$ crystal at room temperature is shown in Fig. 1. The pattern was analyzed using the Topas 2 program. Results obtained show that the as-grown Yb^{3+}:$LiLa(WO_4)_2$ crystal belongs to the tetragonal system with space group I4(1)/a (C_{4h}^6) and unit cell parameters: a_0 = 0.5232 nm and c_0 = 1.1342 nm[12].

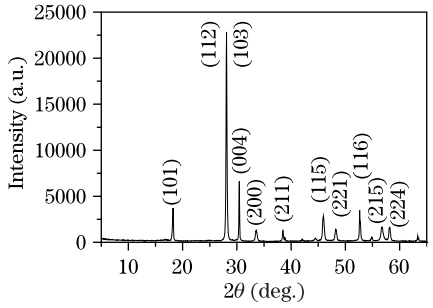

Fig. 1. XRD pattern of as-grown Yb^{3+}:$LiLa(WO_4)_2$ crystal.

The Yb^{3+} concentration on top of the as-grown Yb^{3+}:$LiLa(WO_4)_2$ crystal is 4.28 at.-%. Taking 6.0 at.-% Yb^{3+} concentration in the initial melt into account, the Yb^{3+} segregation coefficient is 0.713, which is less than unity, implying that Yb^{3+} is not distributed uniformly in the $LiLa(WO_4)_2$ crystal. Therefore, a part was cut from the sample in the spectroscopic experiment, ground into powder, and used in the concentration measurement. The Yb^{3+} concentration obtained is determined to be 4.80 at.-% by ICP-AES. Thus, the Yb^{3+} concentration is $2.88\times10^{20}\text{cm}^{-3}$.

Room temperature polarized absorption spectra of Yb^{3+}:$LiLa(WO_4)_2$ crystal (Fig. 2) exhibit three main absorption peaks centering at 934, 962, and 976 nm. The strongest absorption peak is centered at near 976 nm, with linewidths of 10 and 20 nm for π- and σ-polarization, respectively, comparable to those of other Yb^{3+}-doped scheelite tungstate crystals[8] and much larger than that of Yb^{3+}:YAG[1], Yb^{3+}:KReW (Re = Y, Gd, and Lu)[9−11]. Such a broad absorption band means that the Yb^{3+}:$LiLa(WO_4)_2$ crystal is suitable for pumping an InGaAs diode-laser that emits an output of 900 – 1000 nm and is not restricted to the temperature stability of the output wavelength of diode laser. The inhomogeneous broadening behavior probably originates from the disorder structure of Yb^{3+}:$LiLa(WO_4)_2$ crystal. The absorption cross section can be determined by

$$\sigma_{\text{abs}}(\lambda) = k(\lambda)/N_0, \tag{1}$$

where $k(\lambda)$ is the absorption coefficient at the wavelength λ, and N_0 is the Yb^{3+} concentration in the as-grown crystals. Thereby, the absorption cross sections obtained at 976 nm are 2.43×10^{-20} and 1.68×10^{-20} cm^2 for π- and σ-polarization, respectively, smaller than those of Yb^{3+}:KReW[9−11], but comparable to those of other Yb^{3+}-doped scheelite tungstate crystals[8]. This indicates that Yb^{3+}:$LiLa(WO_4)_2$ crystal have strong absorption capability for the pumping light from the InGaAs diode laser.

Polarized fluorescence spectra of Yb^{3+}:$LiLa(WO_4)_2$ crystal at room temperature, as depicted in Fig. 3, show a broad emission band extending from 920 to 1100 nm. Fluorescence spectra linewidths are 59 and 62 nm for π- and σ-polarization, respectively, larger than those of Yb^{3+}:KReW[9−11] and comparable to those of other Yb^{3+}-doped scheelite tungstate crystals[8]. This condition implies that the Yb^{3+}:$LiLa(WO_4)_2$ crystal favors the generation of ultrashort laser pulse.

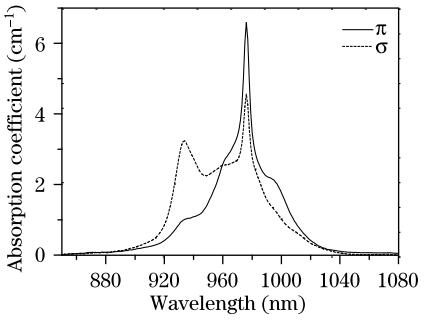

Fig. 2. Polarized absorption spectra of Yb^{3+}:$LiLa(WO_4)_2$ crystal at room temperature.

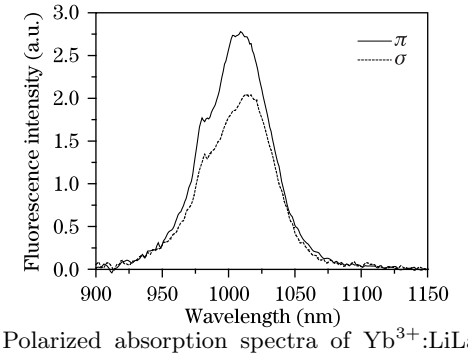

Fig. 3. Polarized absorption spectra of Yb^{3+}:$LiLa(WO_4)_2$ crystal at room temperature.

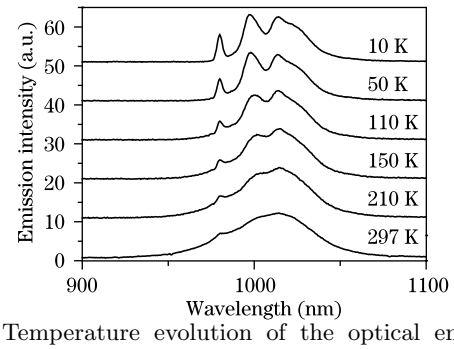

Fig. 4. Temperature evolution of the optical emission of Yb^{3+}:$LiLa(WO_4)_2$ crystal.

Figure 4 shows the temperature evolution of the optical emission of Yb^{3+}:$LiLa(WO_4)_2$ crystal. In the figure, the fluorescence spectral profile changes strongly as the temperature increases. This can be a result of the reabsorption effect related to new transitions from thermally populated ground state sublevels and the broadening of individual linewidths. To our interest, thermal behavior of the fluorescence peak at 997 nm strongly decreases with decreasing temperature. One absorption line with vibronic substructure emerges with increasing temperature in the same spectral position. This line is missing in the absorption spectrum at 10 K[15], the position and thermal evolution of which reveal that this absorption line is from the population of $^2F_{7/2}(1)$ sublevel. The disappearance of the fluorescence line at 997 nm is caused by re-absorption effect.

Based on reciprocity method, the emission cross-section $\sigma_{\text{em}}(\lambda_{\text{ex}})$ at wavelength λ_{ex} can be obtained from the absorption cross-section $\sigma_{\text{abs}}(\lambda_{\text{ex}})$ by the following reciprocity method[1,15,16]:

$$\sigma_{\text{em}}(\lambda_{\text{ex}}) = \sigma_{\text{abs}}(\lambda_{\text{ex}})\frac{Z_{\text{l}}}{Z_{\text{u}}}\exp[(E_{\text{l}} - hc/\lambda_{\text{ex}})/kT], \tag{2}$$

where E_{l} is the zero-line energy defined as the energy separation between the lowest Stark levels of each manifold; kT is 205 cm^{-1} at room temperature; and Z_{l} and Z_{u} are the lower and upper manifold partition functions, respectively, which are given by

$$Z_k = \sum_k d_k \exp(-E_k/kT), \tag{3}$$

where d_k is two due to the Kramers degeneracy, E_k is the lowest excited state energy, which is the energy separation between the lowest components of upper and lower states. With the Stark energy levels of $^2\text{F}_{5/2}$ and

$^2F_{7/2}$ of Yb^{3+} obtained above, Z_l and Z_u are calculated to be 1.6508 and 1.5631, respectively. Thus, the ratio Z_l/Z_u obtained is 1.06, and E_k is equal to 10245.9 cm^{-1} in our case, which almost coincides with the zero-line energy. Thereby, the emission cross sections obtained are 1.63×10^{-20} cm^2 at 1009 nm for π-polarization and 1.53×10^{-20} cm^2 at 1013 nm for σ-polarization, respectively. These are smaller than those of Yb^{3+}:KReW[9−11], but comparable to those reported for other Yb^{3+}-doped scheelite tungstate crystals[8], which is advantageous for Q-switching performance.

The $^2F_{5/2} \rightarrow {}^2F_{7/2}$ transition of Yb^{3+} ions is attributed to a three-level laser system, refractive index of the Yb^{3+}:$LiLa(WO_4)_2$ crystal is relatively large (1.95), the thickness of the sample used is not thin enough (0.5 mm), and a large spectral overlap range (around 950 – 1100 nm) exists between the fluorescence and ground state absorption spectra of the Yb^{3+}:$LiLa(WO_4)_2$ crystal. Thus, the re-absorption phenomenon in Yb^{3+}:$LiLa(WO_4)_2$ bulk crystal is very serious. Fluorescence decay curves in air and alcohol (Fig. 5) exhibit single exponential decay with respective time constants of 1003 and 686 μs, which are longer than the radiative lifetime (356 μs). This further validates the existence of serious re-absorption phenomenon in the Yb^{3+}:$LiLa(WO_4)_2$ bulk crystal. To minimize this self-absorption effect[17,18], room temperature lifetime of the $^2F_{5/2}$ Yb^{3+} multiple is measured on Yb^{3+}:$LiLa(WO_4)_2$ crystal powders dispersed in toluene; a large shift exists between the excitation (λ_{ex} = 930 nm) and the emission (λ_{em} =1020 nm) used. The toluene refractive index $n = 1.495$ decreases the fraction of emission trapped in the particles by the inner reflection. The fluorescence decay curve obtained (Fig. 6) is fitted well by the single exponent, and the fluorescence lifetime obtained is 287 μs. The value is very close to the radiative lifetime.

Yb^{3+}-doped materials produce blue cooperative upconversion when distances between Yb^{3+} ions are small enough to allow interaction between Yb^{3+} ions forming Yb^{3+}-Yb^{3+} pairs. The de-excitation of excited Yb^{3+}-Yb^{3+} pairs results in the emission of a photon at twice the energy of a single ion transition. Cooperative upconversion intensity depends upon the shortest distances between Yb^{3+} ions. In the Yb^{3+}:$LiLa(WO_4)_2$ crystal, the smallest Yb^{3+}-Yb^{3+} distance is 0.3363 nm, implying that it could form an efficient Yb^{3+}-Yb^{3+} pair and there exists cooperative upconversion fluorescence [19−22]. Anti-Stokes fluorescence spectra on 934-nm

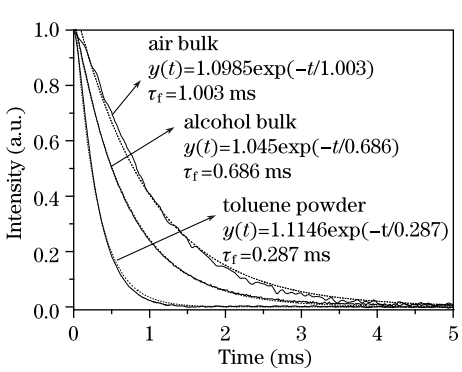

Fig. 5. Fluorescence decay curves of Yb^{3+}:$LiLa(WO_4)_2$ bulk crystal and powder samples.

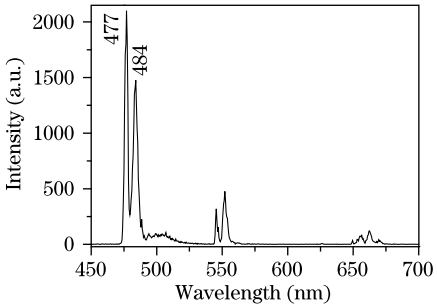

Fig. 6. Anti-Stokes emission spectra of Yb^{3+}:$LiLa(WO_4)_2$ crystal at 10 K.

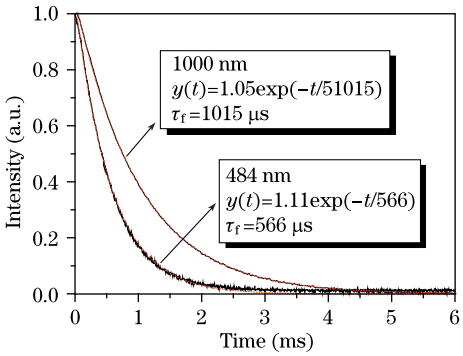

Fig. 7. Fluorescence decay curves of 1000-and 484-nm emissions from Yb^{3+} in $LiLa(WO_4)_2$ crystal at 10 K. The pump wavelength is 934 nm.

excitation at 4 K are shown in Fig. 7. Some peaks are observed in the blue-green emission band, in addition to the red one. The anti-Stokes lines observed at 477 and 484 nm in the range of 470 – 520 nm are believed to be cooperative upconversion caused by simultaneous radiative relaxation of the excited Yb^{3+}-Yb^{3+} pairs accompanied by the emission of a visible photon resulting from $^2F_{5/2}+{}^2F_{5/2} \rightarrow {}^2F_{7/2}+{}^2F_{7/2}+h\nu$[19].

On one hand, according to absorption spectra of the Yb^{3+}:$LiLa(WO_4)_2$ crystal, absorption Stark peak positions of Yb^{3+} ion $^2F_{5/2}$ level are (Yb^{3+}-1^{main}: 976 nm, 10245.9 cm^{-1}), (Yb^{3+}-2^{sub}: 962.0 nm, 10395.0 cm^{-1}), and (Yb^{3+}-3^{sub}: 934.0 nm, 10706.6 cm^{-1}). The Yb^{3+} ion is easily excited to its $^2F_{5/2}$ level from ground level $^2F_{7/2}$ by absorbing a 934-nm (10706.6 cm^{-1}) laser photon. Therefore, if two Yb^{3+} ions happen to form a cluster, the coupled state may be located at 20956.9 cm^{-1} made up of the Yb^{3+} ions' sub-states (Yb^{3+}-1^{main}: 976 nm, 10245.9 cm^{-1}) and (Yb^{3+}-2^{sub}: 934.0 nm, 10706.6 cm^{-1}), which is very close to the measured main peak ($Yb^{3+}Yb^{3+}$-A^{main}: 477 nm, 20952.5 cm^{-1}). Similarly, the coupled state located at 20656.7 cm^{-1} may be made up of the Yb^{3+} ions' sub-states (Yb^{3+}-2^{sub}: 962.0 nm, 10395.0 cm^{-1}) and (Yb^{3+}-1^{main}: 976 nm, 10245.9 cm^{-1}), which is close to the measured sub-peak at 484 nm ($Yb^{3+}Yb^{3+}$-A^{sub}: 484 nm, 20640.9 cm^{-1}). On the other hand, it can be further approved by the fluorescence decay curves at 484- and 1000-nm emissions on 934-nm excitation at 10 K (Fig. 7). The 1000-nm emission exhibits a single exponential decay with a time constant of 1015 μs. The 484-nm emission also decays with a time constant of 566 μs without any rise time. Thereby, the ratio between the fluorescence lifetime of 484- and 1000-nm emissions is nearly 1:2, as expected in the cooperative process.

Therefore, the 478- and 484-nm upconversion emissions are believed to be one kind of cooperative upconversion fluorescence originating from the coupled states of the Yb^{3+}-Yb^{3+} clusters[19−23]. Its mechanism is explained as follows: first, each isolated Yb^{3+} ion absorbs a 934-nm photon and is excited to the $^2F_{5/2}$ state from the $^2F_{7/2}$ ground state; then, both excited state $^2F_{5/2}$ Yb^{3+} ions form a coupled cluster state $^2F^2_{5/2}F_{5/2}$ ($Yb^{3+}Yb^{3+}$) under the laser pumping; the fluorescence at 478 and 485 nm is then radiated by the transition from excited coupled state $^2F_{5/2}$ $^2F_{5/2}$ ($Yb^{3+}Yb^{3+}$) to the ground coupled state $^2F_{7/2}F_{7/2}$ ($Yb^{3+}Yb^{3+}$)[20].

Remaining sharp emission bands in the upconversion emission spectra can be attributed to the anti-Stokes emission of Er^{3+}, Tm^{3+}, or Ho^{3+} involved as impurities in the Yb^{3+}:$LiLa(WO_4)_2$ crystal as a result of Yb^{3+} →Er^{3+}, Yb^{3+} →Tm^{3+}, or Yb^{3+} →Ho^{3+} energy transfer. The emission band in the region of 530 – 570 nm is considered as energy transfer from Yb^{3+} $^2F_{5/2}$ →$^2F_{7/2}$ transition to Er^{3+} $^4I_{11/2}$ →$^4I_{15/2}$ excited state absorption followed by the $^4S_{3/2}$−$^4I_{15/2}$ transition. This band can also originate from $^5I_6$−$^5S_2$ absorption transition followed by the $^5S_2$−$^5I_8$ emission transition of Ho^{3+}. The 630 – 680 nm emission can result from $^4F_{9/2}$-$^4I_{15/2}$ transition of Er^{3+}, $^1G_4$-$^3H_4$ transition of Tm^{3+}, or $^5F_5$-$^5I_8$ transition of Ho^{3+}. As the characteristic absorption peaks of Er^{3+}, Tm^{3+}, or Ho^{3+} impurities are not observed, their concentrations could be very low. The strong intensity of all peaks is noticeable considering that its concentration is probably of traces.

In conclusion, the spectroscopic characteristics and fluorescence dynamics of the Yb^{3+}:$LiLa(WO_4)_2$ crystal are investigated. The strongest absorption peaks with the linewidths of 10 and 20 nm for π- and σ-polarization, respectively, are centered at 976 nm, with the absorption cross-sections of 2.43×10^{-20} and 1.68×10^{-20} cm^2. The broad emission band with a peak at 1020 nm has linewidths of 47 and 45 nm for π- and σ-polarization, respectively, and the corresponding peak emission cross-sections are 1.63×10^{-20} and 1.53×10^{-20} cm^2. Fluorescence lifetime is 287 μs. The 477- and 484-nm cooperative upconversion emissions are observed and demonstrated at 4 K under 934-nm excitation. In comparison with Yb^{3+}-doped crystal materials, Yb^{3+}:$LiLa(WO_4)_2$ crystal is characterized by broad absorption and emission spectra band, as well as large absorption and emission cross sections[8]. Therefore, the Yb^{3+}:$LiLa(WO_4)_2$ crystal may be regarded as a potential tunable laser material.

This work was supported by the National Natural Science Foundation of China (No. 60808033) and the Natural Science Foundation of Jiangxi Province (No. 2008GZW0012).

References

1. L. D. Deloach, S. A. Payne, L. L. Chase, L. K. Smith, W. L. Kang, and W. F. Krupke, IEEE J. Quantum Electron. **29,** 1179 (1993).
2. W. F. Krupke, IEEE J. Sel. Top. Quantum Electron. **6,** 1287 (2000).
3. G. Yao, L. Su, X. Xu, L. Zheng, and J. Xu, Chin. Opt. Lett. **6,** 133 (2008).
4. P. Yan, S. Yin, and M. Gong, Chin. Opt. Lett. **6,** 580 (2008).
5. C. Cascales, M. D. Serrano, F. Esteban-Betegón, C. Zaldo, R. Peters, K. Petermann, G. Huber, L. Ackermann, D. Rytz, C. Dupré, M. Rico, J. Liu, U. Griebner, and V. Petrov, Phys. Rev. B **74,** 174114 (2006).
6. A. García-Cortés, J. M. Cano-Torres, X. Han, C. Cascales, C. Zaldo, X. Mateos, S. Rivier, U. Griebner, V. Petrov, and F. J. Valle, J. Appl. Phys. **101,** 063110 (2007).
7. J. Liu, J. M. Cano-Torres, F. Esteban-Betegón, M. D. Serrano, C. Cascales, C. Zaldo, M. Rico, U. Griebner, and V. Petrov, Opt. Laser Technol. **39,** 558 (2007).
8. A. García-Cortés, J. M. Cano-Torres, M. D. Serrano, C. Cascales, C. Zaldo, S. Rivier, X. Mateos, U. Griebner, and V. Petrov, IEEE J. Quantum Electron. **43,** 758 (2007).
9. X. Huang and G. Wang, Opt. Mater. **31,** 919 (2009).
10. X. Mateos, R. Solé, J. Gavaldà, M. Aguiló, J. Massons, F. Díaz, V. Petrov, and U. Griebner, Opt. Mater. **28,** 519 (2006).
11. M. C. Pujol, M. A. Bursukova, F. Güell, X. Mateos, R. Solé, J. Gavaldà, M. Aguiló, J. Massons, F. Díaz, P. Klopp, U. Griebner, and V. Petrov, Phys. Rev. B **65,** 165121 (2002).
12. N. V. Kuleshov, A. A. Lagatsky, A. V. Podlipensky, V. P. Mikhailov, and G. Huber, Opt. Lett. **22,** 1317 (1997).
13. X. Huang, Z. Lin, Z. Hu, L. Zhang, J. Huang, and G. Wang, J. Cryst. Growth **269,** 401 (2004).
14. X. Huang, Q. Fang, Q. Yu, X. Lü, L. Zhang, Z. Lin, and G. Wang, J. Alloys Comp. **468,** 321 (2009).
15. X. Huang, Z. Lin, Z. Hu, L. Zhang, T. Tsuboi, and G. Wang, Opt. Mater. **29,** 403 (2006).
16. D. E. McCumber, Phys. Rev. **136,** A954 (1964).
17. B. F. Aull and H. P. Jenssen, IEEE J. Quantum Electron. **18,** 925 (1982).
18. J. Liao, Y. Lin, Y. Chen, Z. Luo, E. Ma, X. Gong, Q. Tan, and Y. Huang, J. Opt. Soc. Am. B **23,** 2572 (2006).
19. D. S. Sumida and T. Y. Fan, Opt. Lett. **19,** 1343 (1994).
20. E. Nakazawa and S. Shionoya, Phys. Rev. Lett. **25,** 1710 (1970).
21. D. Deng, S. Xu, R. Bao, S. Zhao, B. Wang, H. Wang, and H. Ju, J. Phys. D: Appl. Phys. **42,** 105111 (2009).
22. M. O. Ramírez, L. E. Bausá, E. Cavalli, and E. Bovero, J. Appl. Phys. **99,** 013507 (2006).
23. G. Boulou, Y. Guyot, H. Canibano, S. Hraiech, and A. Yoshikawa, J. Opt. Soc. Am. B **25,** 884 (2008).